

# Safe Control using Occupancy Grid Map-based Control Barrier Function (OGM-CBF)

Golnaz Raja, Teemu Mökkönen, Reza Ghabcheloo

**Abstract**—Safe navigation in unknown environments stands as a significant challenge in the field of robotics. Control Barrier Function (CBF) is a strong mathematical tool to guarantee safety requirements. However, a common assumption in many works is that the CBF is already known and obstacles have predefined shapes. In this letter, we present a novel method called Occupancy Grid Map-based Control Barrier Function (OGM-CBF), which defines Control Barrier Function based on Occupancy Grid Maps. This enables generalization to unknown environments while generating online local or global maps of the environment using onboard perception sensors such as LiDAR or camera. With this method, the system guarantees safety via a single, continuously differentiable CBF per time step, which can be represented as one constraint in the CBF-QP optimization formulation while having an arbitrary number of obstacles with unknown shapes in the environment. This enables practical real-time implementation of CBF in both unknown and known environments. The efficacy of OGM-CBF is demonstrated in the safe control of an autonomous car in the CARLA simulator and a real-world industrial mobile robot.

**Index Terms**—Autonomous Vehicle Navigation, Collision Avoidance, Vision-Based Navigation, Sensor-based Control.

## I. INTRODUCTION

APPLICATIONS of mobile robots in domains such as autonomous vehicles, industrial robots, and multi-agent systems are often tasked to respect safety while navigating in complex and unknown environments, which stands as one of the most formidable challenges in the field of robotics [1]. One promising approach to integrate safety into design is via Control Barrier Function (CBF) [2] due to the strong mathematical guarantee of satisfying safety requirements. CBFs have been applied in various fields such as legged robots [3], autonomous vehicles [4], multi-robot systems [5] [6], decentralized multi-agent control [7], and drones [8].

In recent years, CBF has been successfully integrated with Control Lyapunov Function (CLF) via Quadratic Programs (QP) for safety critical systems [9], enabling the simultaneous satisfaction of safety and stability. Moreover, given a potentially unsafe nominal control policy, CBF can be embedded as a QP-based safety filter to modify the unsafe control command in a minimally invasive manner to prevent

This work was jointly supported by Academy of Finland (SA) 345517, under SA-NSF joint call on artificial intelligence and wireless communication, and Together for RISC-V Technology and Applications (TRISTAN) under Grant 101095947. (Corresponding author: Golnaz Raja.)

All authors are with the Faculty of Engineering and Natural Sciences, Tampere University, 33720 Tampere, Finland. (e-mail: (golnaz.raja@tuni.fi; teemu.mokkonen@tuni.fi; reza.ghabcheloo@tuni.fi).

violations of the safety constraints [2].

In designing CBF, it is generally assumed that unsafe sets are already known (usually as circular shapes), which is not applicable to unsafe sets with arbitrary shapes in uncharted environments. Practical implementation of CBF in unknown environments relies on a sufficient awareness of the environment, unsafe regions, and their changes to reach a quick, yet smooth generation of a safety certificate as a response. This requires online estimation of unsafe sets and their integration into the CBF formulation.

One practical approach to operate safely in unknown and dynamic environments without sufficient prior information about the environment is the integration of sensory data into the CBF formulation. This enables the online synthesis of CBF based on the aggregated sensor data from perceptive sensors such as LiDAR or camera.

To construct CBF based on sensor data, one approach is to learn both the classification of safe and unsafe regions and CBF simultaneously based on sensor measurements. In [10], the authors used neural networks to learn the CBF directly in the observation space using local observations from LiDAR, without the need for the robot's state estimation and localization. In [11], the authors designed a neural network, called BarrierNet, to learn CBF with respect to the user-defined safe sets, and in [12], a neural network was trained to extract features from front-view images and learn the BarrierNet as an end-to-end vision-based solution for lane keeping and obstacle avoidance. In [13], CBF is synthesized based on the online approximation of the signed distance function from LiDAR measurements using an incremental training approach with replay memory, and in [14], CBF is constructed based on the classification of safe and unsafe sets using a support vector machine on LiDAR measurements. In these approaches, sensor data at each time step is immediately employed to construct CBF, resulting in a lack of historical memory for obstacles that have been previously seen. Moreover, these methods are bound to specific sensor modalities and cannot combine information from different sensors for CBF generation.

One other approach is to distinguish the tasks of classifying safe and unsafe areas from the synthesis of CBF, treating them as separate modules. Consequently, established classification

techniques, such as semantic segmentation and mapping, can be utilized to identify safe and unsafe areas, upon which CBF can be defined. This modular approach can enhance the efficacy of the final controller, particularly in the case of significant changes in the type of environment where the safe controller is deployed. In V-CBF [15], Control Barrier Functions are defined based on segmented unsafe sets using RGBD cameras. Although this framework successfully navigates safely and avoids obstacles with unknown shapes in uncharted environments, it relies solely on instantaneous sensor inputs and lacks memory of previously encountered obstacles. Moreover, as the robot is considered as a point, to cover the size and shape of the robot, a handful of the most conservative points of the constructed CBF should be selected and added as multiple constraints in QP formulation for a successful safe navigation. It is not trivial how these points are selected.

One practical way to approximate the shapes of obstacles is Occupancy Grid Map (OGM). OGM, as a multi-dimensional discrete map, efficiently captures the complexity of the surrounding environment, including the state and shape of all detected obstacles. With accurate state estimation for the robot, the OGM illustrates the relative positions of obstacles with respect to the robot, providing comprehensive situational awareness. The map employs a probabilistic formulation to store all previously seen obstacles, retaining information about these past encounters. Additionally, obstacles within the OGM can be inflated according to the robot's size, enhancing safe navigation. OGM not only embeds essential information for the robot's safe navigation, including the position and inflated shape of obstacles, but it also can be constructed online using real-time sensor data. Online mapping facilitates the robot's navigation in unknown environments since mapping and synthesizing CBFs can be done in real time. Moreover, various sensor configurations can be utilized to generate OGMs, making it a versatile tool for representing unsafe zones. However, OGM alone cannot be directly used for generating CBF since OGM behaves in a binary manner and does not hold correct variational behavior near the boundary of unsafe sets. Thus, a domain translation function is necessary to transform the occupancy grid map into a representation suitable for CBF synthesis. In [16], CBF was designed using elliptical outer approximation on occupancy grid maps. However, the obstacles were approximated with minimum bounding circles, which can be overly conservative. Additionally, this approach requires a separate constraint for each obstacle.

In this paper, we introduce a novel method to define CBF based on occupancy grid maps called Occupancy Grid Map-based Control Barrier Function (OGM-CBF). Our contribution is as follows:

- CBF is represented as a single constraint at each time

step in a QP formulation while assuming the presence of an arbitrary number of obstacles with unknown shapes, enabling real-time and computationally light optimization to guarantee safety.

- The designed safe controller is sensor agnostic. In addition, CBF can be constructed from hybrid sensor modalities using occupancy grid maps.
- The constructed CBF has a memory of all previously seen obstacles.
- The constructed CBF accounts for the size and shape of the robot using an inflated occupancy grid map.
- We evaluated the efficacy of the proposed method in the CARLA simulator in complex scenarios as well as with an industrial mobile robot in real-world experiments.

The outline of this paper is as follows. Section II reviews the principles of Control Barrier Function, Occupancy Grid Map, and Signed Distance Function. Section III describes our designed control methodology. Section IV explains the designed smoothing function used in our CBF. Section V is dedicated to the demonstration of the introduced control strategy in the CARLA simulator and on a real robot. Finally, in section VI, the conclusions and future work are provided.

## II. PRELIMINARIES AND BACKGROUND

Consider a non-linear control-affine system:

$$\begin{aligned}\dot{\mathbf{x}} &= f(\mathbf{x}) + g(\mathbf{x})\mathbf{u} \\ z &= O(\mathbf{x}, \mathbf{q})\end{aligned}\quad (1)$$

where  $\mathbf{x} \in \mathbb{X} \subseteq \mathbb{R}^n$ ,  $f : \mathbb{R}^n \rightarrow \mathbb{R}^n$  and  $g : \mathbb{R}^n \rightarrow \mathbb{R}^2$  are locally Lipschitz continuous functions,  $O : \mathbb{R}^n \times \mathbb{R}^q \rightarrow \mathbb{R}^k$  is a perception sensor module such as camera or LiDAR capable of generating occupancy grid maps,  $\mathbf{x}$  and  $z$  are the state and observation vectors, respectively, and  $\mathbf{q}$  is environment variables. In this paper, our system is a kinematic model of a robot with  $\mathbf{u} = [v, \omega]^T$ , the linear and angular speeds as input.

*Definition 1 (Local Lipschitz continuity):* Let  $f : D \subseteq \mathbb{R}^n \rightarrow \mathbb{R}^m$  be a function.  $f$  is locally Lipschitz continuous at a point  $x \in D$  if there exist constants  $M > 0$  and  $\delta > 0$  such that for all  $x' \in D$  with  $\|x - x'\| \leq \delta$ , the inequality  $\|f(x) - f(x')\| \leq M\|x - x'\|$  is satisfied.

### A. Control Barrier Function

In this paper, we define the safe system as follows:

*Definition 2 (Safe system):* The system (1) is categorized as safe if  $\mathbf{x}(t) \in \mathbb{X}_s \subseteq \mathbb{X}$ ,  $\mathbf{u}(t) \in \mathbb{U}_s \subseteq \mathbb{U}$ ,  $\forall t \geq 0$ . Where  $\mathbb{X}_s$  is the set of safe states, and  $\mathbb{U}_s$  is the set of admissible control inputs.

Consider  $S \subseteq \mathbb{X}_s$  to be zero-superlevel set of a continuously differentiable function  $h(\mathbf{x}) : \mathbb{X} \rightarrow \mathbb{R}$ , yielding:

$$S = \{\mathbf{x} \in \mathbb{X} \mid h(\mathbf{x}) \geq 0\} \quad (2)$$

To keep the system (1) remain in the safe set for all time, the set  $S$  should be a forward invariant set.

*Definition 3 (Forward invariant set):* A set  $S$  is forward invariant set for the control system (1) if state trajectories starting in  $S$  will remain in  $S$  for the future time. That is, if  $\mathbf{x}(0) \in S$ , there exists  $\mathbf{u}(t) \in \mathbb{U}_s \subseteq \mathbb{U}$ , such that  $\mathbf{x}(t) \in S$ ,  $\forall t \geq 0$  [17].

As proven in [2], given the dynamic system (1), the function  $h(\mathbf{x})$  is a control barrier function if there exists an extended class  $\kappa$  function  $\alpha(\cdot)$  such that for all  $\mathbf{x} \in \mathbb{X}$ :

$$\sup_{\mathbf{u} \in \mathbb{U}_s} \left[ \frac{\partial h(\mathbf{x})}{\partial \mathbf{x}} (f(\mathbf{x}) + g(\mathbf{x})\mathbf{u}) \right] \geq -\alpha(h(\mathbf{x})). \quad (3)$$

We will later use  $\dot{h}(\mathbf{x}, \mathbf{u}) = \frac{\partial h(\mathbf{x})}{\partial \mathbf{x}} (f(\mathbf{x}) + g(\mathbf{x})\mathbf{u})$  notation for brevity.

*Definition 4 (Extended class  $\kappa$  function):* An extended class  $\kappa$  function is a function  $\alpha : \mathbb{R} \rightarrow \mathbb{R}$  that is strictly increasing and  $\alpha(0) = 0$ .

### B. Occupancy Grid Map

Occupancy grid maps (OGMs) are fundamental tools in mobile robotics for mapping and navigation. They represent the environment as a tessellated, multi-dimensional grid, with each cell quantifying whether a part of the environment is occupied or not [18]. This setup, given the state of the system, incorporates a probabilistic approach to account for uncertainties in measurements and the robot's pose estimation [19], [20]. OGMs are typically updated using sensor data from LiDAR, sonar, or vision systems and the robot's movements over time. This process can be employed using various frameworks, including probabilistic [18], Bayesian [21], neural network-based [22], and forward modeling approaches [23].

The process of dynamically generating an occupancy grid map based on the current robot state and sensor inputs can be succinctly described as follows:

$$m' = M(\mathbf{x}, z, m), \quad (4)$$

where  $\mathbf{x}$  represents the robot's current state,  $z$  denotes the measurements from onboard perception sensors, and  $m$  is the existing map. The function  $M : \mathbb{R}^n \times \mathbb{R}^k \times \mathbb{R}^p \rightarrow \mathbb{R}^p$  updates the current map belief  $m$  to  $m'$ , by integrating new sensor data at the latest state of the robot into the map.

This formulation reflects that the occupancy grid map continuously evolves, capturing real-time changes in the environment as detected by the sensors and the movement of the robot.

In this paper, the occupancy grid map  $m$  is converted into a binary representation. In the binary OGM, each occupied cell signifies an obstacle in the environment. Consequently, the overall unsafe set, denoted by  $\mathbb{X}_u$ , is defined as the union of all states corresponding to the occupied cells of the map. Trivially,

the final safe set  $\mathbb{X}_s$  is given by  $\mathbb{X} \setminus \mathbb{X}_u$ , which includes all states where the robot is located in non-occupied cells of the map. The process of deriving the safe set  $\mathbb{X}_s$  from map  $m$  can be described briefly as follows:

$$\mathbb{X}_s = M_b(m) \quad (5)$$

### C. Signed Distance Function

A signed distance function (SDF) is a function that, for a given point  $p$ , outputs the signed distance from  $p$  to the closest boundary of a set  $\Omega$  in a metric space. The sign of the distance indicates whether  $p$  is inside or outside  $\Omega$  [24]. In this paper, this function is defined to take positive values for points inside  $\Omega$ , decrease in value as  $p$  approaches the boundary where the distance is zero, and take negative values outside  $\Omega$ . If  $\Omega$  is a subset of a metric space with metric  $d$ , the described signed distance function is defined as follows:

$$\phi(p, \Omega) \equiv \begin{cases} d(p, \partial\Omega) & \text{if } p \in \Omega \\ -d(p, \partial\Omega) & \text{if } p \notin \Omega \end{cases} \quad (6a)$$

where  $\partial\Omega$  denotes the boundary of the set  $\Omega$  and  $d(p, \partial\Omega)$  represents the minimum distance from  $p$  to points on the boundary. Additionally,  $d(\cdot, \partial\Omega)$  is the desired distance metric to the set  $\partial\Omega$ .

In the case where  $\Omega$  is a subset of Euclidean space  $\mathbb{R}^n$  with a piecewise smooth boundary, and  $d(\cdot, \partial\Omega)$  is the Euclidean distance metric, the signed distance function is differentiable almost everywhere. Moreover, the gradient of the function satisfies the eikonal equation  $|\nabla\phi| = 1$  at every point where it is differentiable [25].

## III. CONTROL METHODOLOGY

In this section, we introduce a novel method for defining CBF using occupancy grid maps. Like traditional CBFs, the designed CBF can be applied using various formulations, such as a safety filter or a CBF-CLF QP. For our experimental evaluations, we have chosen the CBF-CLF QP formulation. Essential details of this formulation are succinctly provided in this section.

### A. Occupancy Grid Map-based Control Barrier Function (OGM-CBF)

Assuming the online occupancy grid map  $m$  updating as defined in (4), we will show that the safety is achieved using a control barrier function defined as follows:

$$h(\mathbf{x}) = \Phi_s(\mathbf{x}, m) + l_s + l_a \cos(\eta) \quad (7)$$

where:

- $\Phi_s(\mathbf{x}, m) = T(\phi(\mathbf{x}, M_b(m)))$ , and  $T : \mathbb{R} \rightarrow \mathbb{R}$  is a scalar odd function for shaping and smoothing. In other words,  $\Phi_s$  is a smoothed signed distance function of the set  $\mathbb{X}_s$ , evaluated at the robot's body frame position  $p$  in the map, noting that  $p$  is part of the state vector  $\mathbf{x}$ .

- $\eta$  is the angle between vectors  $\hat{x}$ , and  $\nabla_p \Phi_s(\mathbf{x}, m)$ , where  $\hat{x}$  is the unit vector of the first coordinate of the body frame,  $\nabla_p \Phi_s(\mathbf{x}, m)$  is gradient of  $\Phi_s(\mathbf{x}, m)$ .
- $l_s$ , and  $l_a$  are scalar values such that  $0 < l_a \leq -l_s$ .

Note that in above equations, all the quantities such as body frame and map frame, and accordingly  $\Phi_s$  are defined in the same coordinate frame, for instance, the robot ego-centric frame.

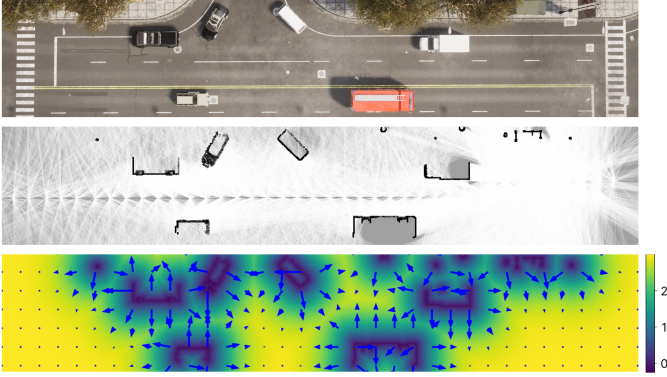


Fig. 1. Top-view snapshot of the environment in CARLA. The second row shows the constructed occupancy grid map, and the last row shows  $\Phi_s(\mathbf{x}, m)$  and its gradient field in the map frame for all the states in the map.

Next, we provide some intuition of the proposed CBF in (7). The proposed CBF function comprises two main components: i) the effect of the robot's distance to obstacles, and ii) the angle between the robot's heading and the gradient of the SDF function  $\Phi_s$ .

In the first component,  $\Phi_s(\mathbf{x}, m)$ , map  $m$  captures the latest location, shape, and size of the obstacles within the map at each time step, as outlined in (4). In the map, each occupied cell indicates an obstacle. Although effective, this map lacks smooth transitional values. In Fig. 1, the top row displays a top view of the scenario and obstacle status, while the second row depicts the resulting binary occupancy grid map. Function  $\phi$  is smooth almost everywhere except at the curves where the closest obstacle region switches. Applying  $T(\cdot)$  to  $\phi$  ensures smooth  $\Phi_s$  everywhere. The last row in Fig. 1 illustrates the smooth  $\Phi_s$  in the map coordinate.

The second component,  $l_s + l_a \cos(\eta)$ , involves calculating the cosine similarity between two vectors:  $\hat{x}$ , representing the robot heading, and  $\nabla_p \Phi_s(\mathbf{x}, m)$ . Notice that  $\nabla_p \Phi_s$  is the direction that  $\Phi_s$  increases the most, thus moving in that direction will move the robot further away from obstacles. The gradient field depicted in the last row of Fig. 1 visualizes  $\nabla_p \Phi_s(\mathbf{x}, m)$  within the map frame. Notice that  $l_s$  is a negative number and the value  $-l_s - l_a \geq 0$  is the safety margin, a design choice.

Now, we can establish how the constructed function has the necessary properties to be a control barrier function.

*Theorem 1:* Set  $S = \{\mathbf{x} \in \mathbb{X} \mid h(\mathbf{x}) \geq 0\}$  with  $h(\mathbf{x})$  defined in (7) is a forward-invariant set and  $h(\mathbf{x})$  is a control barrier function for system (1), with  $\mathbf{u} = [v, \omega]^T$  as the control input.

*Proof:* We will first show that  $S \subseteq \mathbb{X}_s$ . The condition  $0 < l_a \leq -l_s$  ensures that  $\forall \mathbf{x}$  we have  $l_s + l_a \cos(\eta) \leq 0$ . For any  $\mathbf{x} \in S = \{\mathbf{x} : h(\mathbf{x}) \geq 0\}$ , we have  $h(\mathbf{x}) \geq 0$ , therefore  $\Phi_s(\mathbf{x}) \geq 0$ , and consequently  $\phi(\mathbf{x}) \geq 0$ , since  $T(\cdot)$  is an odd function. Thus  $\mathbf{x} \in \mathbb{X}_s = \{\mathbf{x} : \phi(\mathbf{x}) \geq 0\}$ , and we have shown the first part.

We will now show that there are control signals  $\mathbf{u}$  such that (3) is satisfied. It is easy to see that  $\dot{h} = \frac{\partial \Phi_s}{\partial \mathbf{x}} \dot{p} + l_a \sin(\eta) \dot{\eta}$ , which can be written as  $\dot{h} = a(\mathbf{x})v + b(\mathbf{x})\omega$ , noting that  $\dot{p}$  and  $\dot{\eta}$  provide the  $v$  term, while  $\dot{\eta}$  provides the  $\omega$  term, assuming a kinematic model. Since  $(v, \omega)$  can be made zero, condition (3) can be satisfied and thus  $h(\mathbf{x})$  is a control barrier function for (1), and  $S$  is an invariant set. ■

Considering the control system in (1), with control inputs  $\mathbf{u} = [v, \omega]^T$ , the control policy outlined in (8) ensures safety across all trajectories originating within  $S$ .

$$\pi_{ogm-cbf} = \{\mathbf{u} \in \mathbb{U} \mid \dot{h}(\mathbf{x}, \mathbf{u}) \geq -\alpha(h(\mathbf{x}))\} \quad (8)$$

It is important to recognize that the efficacy of the safety controller is influenced by the configuration of the function  $T(\cdot)$ ,  $\alpha(\cdot)$ , and the values of  $l_s$ , and  $l_a$ . which can be adjusted according to the model of the system, the dimensions of the map, and the environment.

Note that since the union of all occupied cells is considered in the function  $h(\mathbf{x})$ , and the distance to the closest occupied cell is being calculated in this function, the OGM-CBF automatically will find the arbitrary safe set  $S$ , that considers all the detected obstacles. This means, in contrast to other methods, one CBF construction is enough at each timestep to guarantee staying in the safe set  $S$ , which makes this method computationally efficient.

### B. Including Robot shape in OGM-CBF

OGM-CBF is capable of considering the robot's size and shape using established inflation methods on occupancy grid maps. For example, the robot can be modeled as a union of multiple spheres, similar to that described in [26]. In addition, the occupied cells in the map can be inflated by the radius of the spheres. Then the designed CBF can be analyzed at the centers of these spheres.

One can also choose number of points at the boundary of the robot to be avoided, with one constraint per point in OGM-CBF. Having enough points, the OGM-CBF ensures that the entire boundary of the robot remains within the safe set  $S$ .

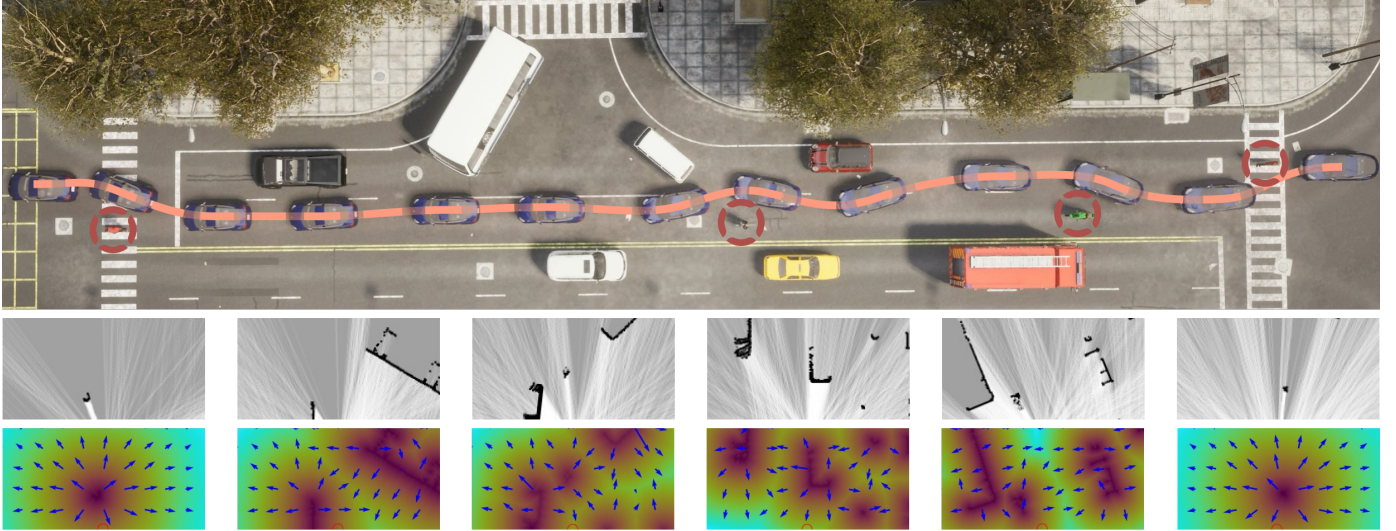


Fig. 2. Top-view snapshot of simulation in the CARLA environment. The blue car is a self-driving vehicle using OGM-CBF to navigate safely. The orange dashed line is the path of the autonomous car. The second row shows the upper half of the ego-centric local occupancy grid map denoted as  $m$ , and the last line illustrates  $\Phi_s(\mathbf{x}, m)$  and its gradient field in the map frame for all the states in the map.

### C. Control Lyapunov Function (CLF)

In addition to ensuring safety, it is imperative to establish a control objective. Consider a candidate Control Lyapunov Function (CLF) for this purpose, denoted as  $V : \mathbb{X} \rightarrow \mathbb{R}$ , characterized by continuous differentiability and positive definiteness.

*Definition 5:* Consider a function  $V : \mathbb{X} \rightarrow \mathbb{R}$  to be positive-definite over the domain  $\mathbb{X}$  provided that: (i)  $V(0) = 0$ , and (ii) for any  $\mathbf{x} \in \mathbb{X}$  with  $\mathbf{x} \neq 0$ , it holds that  $V(\mathbf{x}) > 0$ .

As mentioned in [2], the stability of (1) in equilibrium point can be achieved with a necessary and sufficient condition as follows:

$$\inf_{\mathbf{u} \in \mathbb{U}} [\dot{V}(\mathbf{x}, \mathbf{u}) = \frac{\partial V}{\partial \mathbf{x}}(f(\mathbf{x}) + g(\mathbf{x})\mathbf{u})] \leq -\gamma(V(\mathbf{x})) \quad (9)$$

where  $\gamma(\cdot)$  is defined as an extended class  $\kappa$  function. Consequently, the subsequent control strategy will ensure the stability requirements:

$$\pi_{clf} = \{\mathbf{u} \in \mathbb{U}_s \mid \dot{V}(\mathbf{x}, \mathbf{u}) \leq -\gamma(V(\mathbf{x}))\} \quad (10)$$

### D. Integrating CLF and OGM-CBF

In order to fulfill the criteria for both safety and stability, the proposed control policy should represent the intersection of two preceding policies, denoted as  $\pi^* = \pi_{ogm-cbf} \cap \pi_{clf}$ . In instances where this intersection is empty, prioritization of safety becomes imperative. Consequently, the following constrained optimization problem can be defined to find an optimal control input that simultaneously satisfies the constraints related to safety and stability, respectively as hard and

soft constraints.

$$\mathbf{u}^* = \underset{\mathbf{u}}{\operatorname{argmin}} J(\mathbf{u}) \quad (11a)$$

$$\text{s.t.} \quad \dot{V}(\mathbf{x}, \mathbf{u}) \leq -\gamma(V(\mathbf{x})) + \delta \quad (11b)$$

$$\dot{h}(\mathbf{x}, \mathbf{u}) \geq -\alpha(h(\mathbf{x})) \quad (11c)$$

$$\mathbf{u}_{lb} \leq \mathbf{u} \leq \mathbf{u}_{ub} \quad (11d)$$

where  $J$  represents the cost function, while  $\mathbf{u}_{lb}$  and  $\mathbf{u}_{ub}$  are the lower and upper bounds of the control input, respectively. Additionally,  $\delta$  is identified as the relaxation parameter, which is engaged when the constraints are in conflict, leading to an absence of elements in the intersection  $\pi_{ogm-cbf} \cap \pi_{clf}$ . Under such circumstances, the hard constraint (related to safety) is maintained, whereas the soft constraint (related to stability) is moderated. It is customary to set a quadratic cost  $J(\mathbf{u})$ , which renders the optimization a Quadratic Programs (QP), since the constraints are linear in control  $\mathbf{u}$ .

In the Algorithm (1) steps of deployment of the proposed map-based safe control is expressed.

---

#### Algorithm 1: Map-based Safety Control Algorithm

---

**Input:** sensor data:  $z$ , state of the system:  $\mathbf{x}$

**Output:** Control Input:  $\mathbf{u}$

- 1 **while** Robot is running **do**
  - 2     receive sensor data  $z$  and state of the system  $\mathbf{x}$
  - 3     generate occupancy grid map  $m$
  - 4     generate  $\Phi_s(\mathbf{x}, m)$  and its gradient
  - 5     calculate  $h(\mathbf{x})$ , and  $\dot{h}(\mathbf{x}, \mathbf{u})$  for the current state of the robot
  - 6     run optimization (11) to obtain control inputs:  $\mathbf{u}^*$
-

#### IV. FUNCTION SHAPING AND SMOOTHING

In this section, we aim to explore the properties of the function  $T(\cdot)$  used in generating  $h(\mathbf{x})$  as a control barrier function. Given that the signed distance function is continuously differentiable almost everywhere, as discussed in section II-C, the design of  $T(\phi(\mathbf{x}, M_b(m)))$  ensures that  $h(\mathbf{x})$  maintains continuous differentiability across the entire state space. Notably,  $\phi(\cdot)$  may lack differentiability at non-smooth points or centers of the set  $\Omega$ . To address this,  $T(\phi(\mathbf{x}, M_b(m)))$  translates the grid map values of  $\phi(\mathbf{x}, M_b(m))$  to the state space and employs polynomial interpolation  $p(\cdot)$ , thus guaranteeing continuous differentiability at all points in the state space. This approach ensures that  $h(\mathbf{x})$  is a continuously differentiable function, which is required as specified in (2). As stated before, care needs to be taken as  $T(\cdot)$  needs to be an odd function.

Moreover,  $T(\cdot)$  enhances the control over the shape of  $h(\mathbf{x})$  by adjusting the gradient behaviors and scaling the values of  $\phi(\mathbf{x}, M_b(m))$  through non-linear modifications prior to polynomial interpolation. This adjustment is tailored to fit the dynamics of the system described in (1).

#### V. EXPERIMENTAL EVALUATION

In this section, we will demonstrate the effectiveness of the introduced control strategy on a self-driving car in the CARLA autonomous driving simulator [27] and on an industrial mobile robot.

##### A. CARLA

The experiment aims to validate the safe navigation of an autonomous car using OGM-CBF in a scenario including diverse obstacles. The control inputs are  $\mathbf{u} = [v, \omega]^T$ , and steering and throttle commands are calculated using the standard kinematic bicycle model in a 2D workspace [28]. A LiDAR sensor is mounted on the ego vehicle to generate the occupancy grid map  $m$  online, where each grid cell represents a 0.1 by 0.1 meter area of the environment. The simulation involves navigating an unknown environment cluttered with various stationary obstacles, such as cars and pedestrians.

In this experiment, safe navigation is deployed by a controller based on Algorithm (1), where a quadratic Lyapunov function is used to align the vehicle's heading with a target heading, while the optimization's cost function maintains a desired speed  $v_d = 2m/s$ . The controller's effectiveness can be inspected from Fig. 2. In this Figure, in the first row, the orange line shows the path of the ego vehicle. In addition to cars, smaller obstacles such as pedestrians, bicyclists, and motorcyclists are spawned in the environment (marked with red circles). The second row illustrates the upper half of the ego-centric local occupancy grid map  $m$  during the experiment, and the last row displays  $\Phi_s(\mathbf{x}, m)$  and the gradient field of it in the map frame for all the states in the map. It should be noted that in Fig. 2,

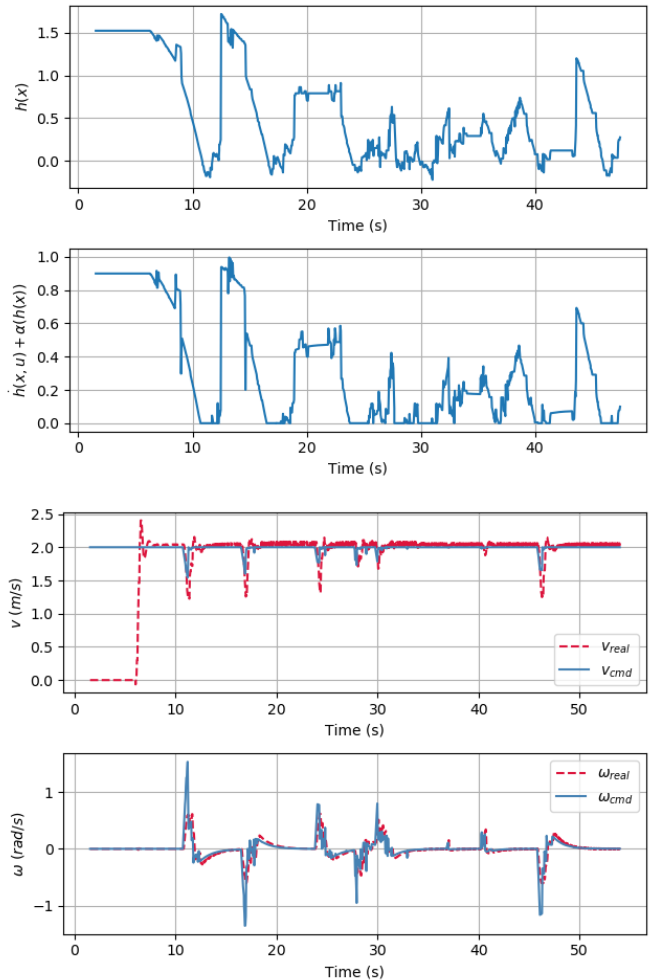


Fig. 3.  $h(\mathbf{x})$  (first),  $\dot{h}(\mathbf{x}, \mathbf{u}) + \alpha(h(\mathbf{x}))$  (second), Linear (third) and angular velocity (forth) of the autonomous vehicle vs. time in the CARLA simulator. The devised commands by the controller are visualized with a solid line, while real measurements are shown using a dashed line.

the ego vehicle initiates its journey from the right side of the page and proceeds towards the left. Additionally, as the robot has a positive lower bound velocity,  $T(\phi(\mathbf{x}, M_b(m)))$  is only constructed for the upper half of the ego-centric map as the function  $p(a \tanh(b\phi(\mathbf{x}, M_b(m))))$ , where  $a$  and  $b$  are tuned based on the desired behaviour, and  $p(\cdot)$  is a polynomial interpolation function as described in section IV.

Fig. 3 quantitatively illustrates that the designed controller in fact navigates safely during the experiment. The first row displays the value of  $h(\mathbf{x})$ , and the second row shows  $\dot{h}(\mathbf{x}, \mathbf{u}) + \alpha(h(\mathbf{x}))$ , which remains non-negative, indicating constant satisfaction of the safety constraint. The third and fourth rows depict the control inputs  $\mathbf{u} = [v, \omega]^T$  generated by Algorithm (1) (solid lines), alongside the actual linear and angular velocities of the vehicle (dashed lines) with respect to time. Note the value of  $h(\mathbf{x})$  can become negative near obstacles due to the approximation of the system (1) as a

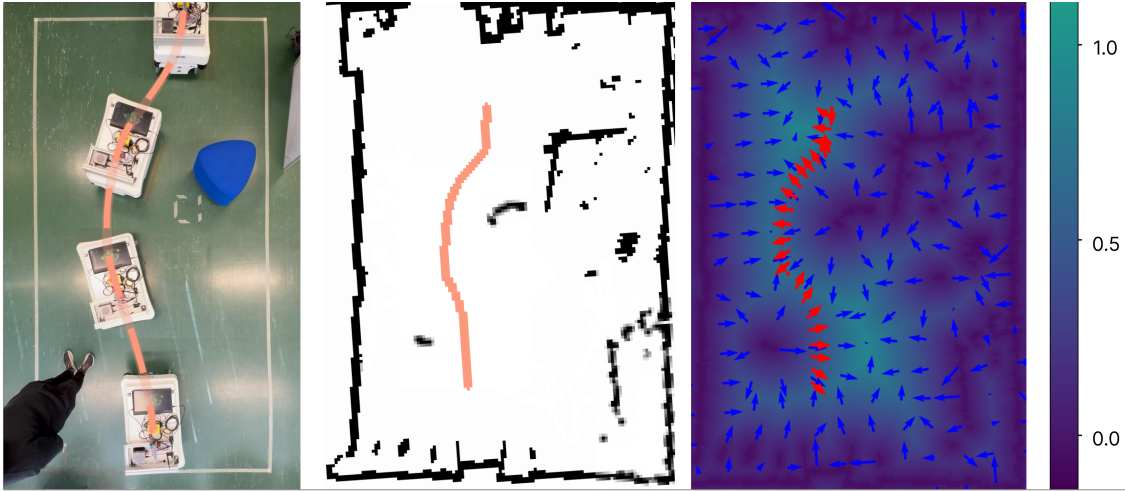


Fig. 4. 2D snapshot of the robot during the experiment (left), the constructed occupancy grid map using onboard sensors (middle), and  $\Phi_s(\mathbf{x}, m)$  and its gradient field in the map frame for all the states in the map (right). The orange line shows the path of the robot and the red gradients are the taken gradient values to the algorithm during the experiment.

kinematic model.

### B. Real-world

Besides simulated validation, additional experiments were conducted on an industrial mobile robot (MiR100), which is a differential wheeled robot equipped with an Nvidia Jetson AGX Orin and two laser scanners. Mapping and safe control are deployed using the ROS2 framework on this platform, and localization is done internally using onboard sensors.

In this experiment, the robot utilizes a pre-established global map of the environment, which is dynamically updated with an average frequency of 16.372 Hz using real-time sensor measurements collected from laser scanners. Each grid cell in the map covers a 0.05 by 0.05 meter section of the environment. Safe navigation is managed by a controller based on Algorithm (1) using OGM-CBF, with a quadratic Lyapunov function for maintaining the desired heading. Moreover, the optimization's cost function is designed to keep the speed of the robot at  $v_d = 0.25$  m/s. The employed controller runs on the platform with an average frequency of 12.498 Hz, and the applied function  $T(\phi(\mathbf{x}, M_b(m)))$  is the same as in the CARLA experiments.

Fig. 4 shows the robot's path (orange lines) during the experiment. The left image demonstrates OGM-CBF's capabilities to avoid obstacles with arbitrary shapes (the blue obstacle and a human). The middle image shows the global occupancy grid map updated in real-time by laser scanners, and the robot's path in the map frame. The right image presents  $\Phi_s(\mathbf{x}, m)$  and its gradient field in the map frame for all the states in the map (blue arrows). Moreover, the gradients of  $\Phi_s(\mathbf{x}, m)$  along the robot's path are marked by red arrows, indicating the direction of avoidance near obstacles utilized in the controller. Note that the robot progresses from

the top to the bottom of the images throughout the experiment.

Fig. 5 quantitatively validates the robot's safe navigation using OGM-CBF during the experiment. The first row displays the value of  $h(\mathbf{x})$ , the second row presents  $\dot{h}(\mathbf{x}, \mathbf{u}) + \alpha(h(\mathbf{x}))$ , and the final two rows illustrate the commanded (solid blue line) and actual (dashed red line) linear and angular velocities of the robot with respect to time.

As values in Fig. 5 illustrate, the robot is able to satisfy the safety constraint of OGM-CBF and navigate safely in the environment. Note that as the system (1) is considered kinematically,  $h(\mathbf{x})$  goes to negative values in proximity to obstacles. However, the controller increases the value of  $h(\mathbf{x})$  successfully by generating proper control commands.

## VI. CONCLUSION

This paper introduces a novel method, the Occupancy Grid Map-based Control Barrier Function (OGM-CBF), which enhances safe navigation in robotics across both known and unknown terrains. By integrating the Control Barrier Function (CBF) with occupancy grid maps, our approach effectively accommodates arbitrary obstacle shapes and configurations. The designed CBF is sensor-agnostic and can be implemented using a range of hybrid sensor modalities. Moreover, the OGM-CBF is formulated as a single constraint in a Quadratic Programming (QP) formulation, taking into account all previously seen obstacles. Additionally, the constructed CBF considers the robot's size while applying established inflation methods to the occupancy grid map.

We validated the effectiveness of OGM-CBF through experiments in the CARLA simulator and practical implementations on an industrial mobile robot, confirming its capability for reliable autonomous navigation. Future work will demonstrate

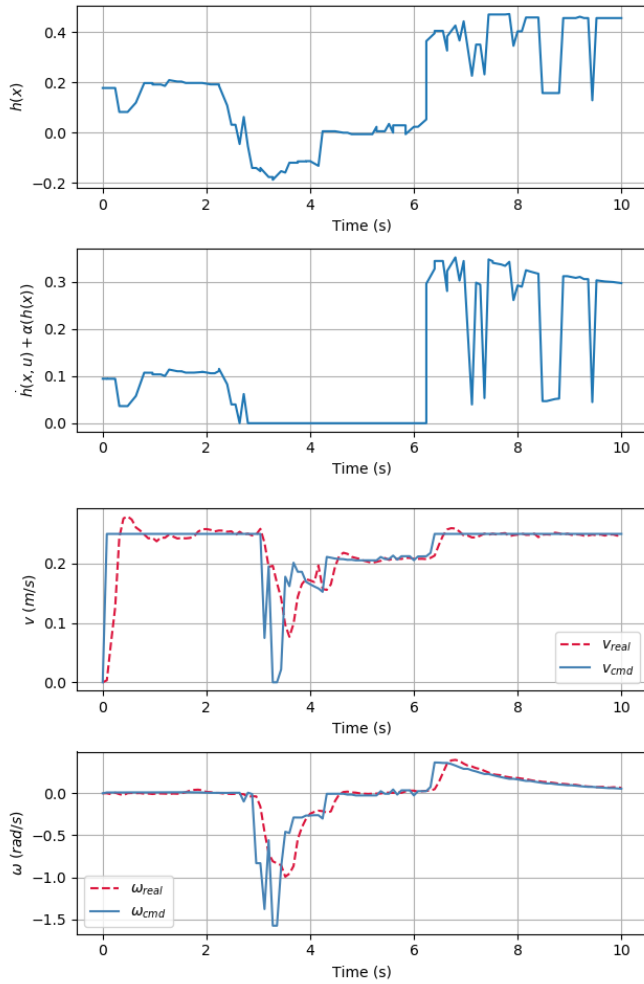


Fig. 5.  $h(\mathbf{x})$  (first),  $\dot{h}(\mathbf{x}, \mathbf{u}) + \alpha(h(\mathbf{x}))$  (second), Linear (third) and angular velocity (forth) of the mobile robot vs. time. The controller's commands are displayed using a solid line, whereas the real measurements are indicated with a dashed line.

the integration of different sensor modalities where safe/unsafe segmentation is integrated to one OGM, and incorporate the effect of the actuator dynamics into the CBF design.

#### REFERENCES

- [1] G.-Z. Yang, J. Bellingham, P. E. Dupont, P. Fischer, L. Floridi, R. Full, N. Jacobstein, V. Kumar, M. McNutt, R. Merrifield, *et al.*, "The grand challenges of science robotics," *Science robotics*, vol. 3, no. 14, p. eaar7650, 2018.
- [2] A. D. Ames, S. Coogan, M. Egerstedt, G. Notomista, K. Sreenath, and P. Tabuada, "Control barrier functions: Theory and applications," in *2019 18th European control conference (ECC)*, pp. 3420–3431, IEEE, 2019.
- [3] Q. Nguyen, A. Hereid, J. W. Grizzle, A. D. Ames, and K. Sreenath, "3d dynamic walking on stepping stones with control barrier functions," in *2016 IEEE 55th Conference on Decision and Control (CDC)*, pp. 827–834, IEEE, 2016.
- [4] A. D. Ames, J. W. Grizzle, and P. Tabuada, "Control barrier function based quadratic programs with application to adaptive cruise control," in *53rd IEEE Conference on Decision and Control*, pp. 6271–6278, IEEE, 2014.
- [5] L. Wang, A. D. Ames, and M. Egerstedt, "Safety barrier certificates for collisions-free multirobot systems," *IEEE Transactions on Robotics*, vol. 33, no. 3, pp. 661–674, 2017.

- [6] Y. Chen, A. Singletary, and A. D. Ames, "Guaranteed obstacle avoidance for multi-robot operations with limited actuation: A control barrier function approach," *IEEE Control Systems Letters*, vol. 5, no. 1, pp. 127–132, 2020.
- [7] Z. Qin, K. Zhang, Y. Chen, J. Chen, and C. Fan, "Learning safe multi-agent control with decentralized neural barrier certificates," *arXiv preprint arXiv:2101.05436*, 2021.
- [8] A. Singletary, A. Swann, Y. Chen, and A. D. Ames, "Onboard safety guarantees for racing drones: High-speed geofencing with control barrier functions," *IEEE Robotics and Automation Letters*, vol. 7, no. 2, pp. 2897–2904, 2022.
- [9] A. D. Ames, X. Xu, J. W. Grizzle, and P. Tabuada, "Control barrier function based quadratic programs for safety critical systems," *IEEE Transactions on Automatic Control*, vol. 62, no. 8, pp. 3861–3876, 2016.
- [10] C. Dawson, B. Lowenkamp, D. Goff, and C. Fan, "Learning safe, generalizable perception-based hybrid control with certificates," *IEEE Robotics and Automation Letters*, vol. 7, no. 2, pp. 1904–1911, 2022.
- [11] W. Xiao, T.-H. Wang, R. Hasani, M. Chahine, A. Amini, X. Li, and D. Rus, "Barriernet: Differentiable control barrier functions for learning of safe robot control," *IEEE Transactions on Robotics*, 2023.
- [12] W. Xiao, T.-H. Wang, M. Chahine, A. Amini, R. Hasani, and D. Rus, "Differentiable control barrier functions for vision-based end-to-end autonomous driving," *arXiv preprint arXiv:2203.02401*, 2022.
- [13] K. Long, C. Qian, J. Cortés, and N. Atanasov, "Learning barrier functions with memory for robust safe navigation," *IEEE Robotics and Automation Letters*, vol. 6, no. 3, pp. 4931–4938, 2021.
- [14] M. Srinivasan, A. Dabholkar, S. Coogan, and P. A. Vela, "Synthesis of control barrier functions using a supervised machine learning approach," in *2020 IEEE/RSJ International Conference on Intelligent Robots and Systems (IROS)*, pp. 7139–7145, IEEE, 2020.
- [15] H. Abdi, G. Raja, and R. Ghabcheloo, "Safe control using vision-based control barrier function (v-cbf)," in *2023 IEEE International Conference on Robotics and Automation (ICRA)*, pp. 782–788, IEEE, 2023.
- [16] J. Liu, M. Li, J. W. Grizzle, and J.-K. Huang, "Clf-cbf constraints for real-time avoidance of multiple obstacles in bipedal locomotion and navigation," in *2023 IEEE/RSJ International Conference on Intelligent Robots and Systems (IROS)*, pp. 10497–10504, IEEE, 2023.
- [17] F. Blanchini, "Set invariance in control," *Automatica*, vol. 35, no. 11, pp. 1747–1767, 1999.
- [18] H. Moravec and A. Elfes, "High resolution maps from wide angle sonar," in *Proceedings. 1985 IEEE international conference on robotics and automation*, vol. 2, pp. 116–121, IEEE, 1985.
- [19] G. N. DeSouza and A. C. Kak, "Vision for mobile robot navigation: A survey," *IEEE transactions on pattern analysis and machine intelligence*, vol. 24, no. 2, pp. 237–267, 2002.
- [20] T. Collins and J. Collins, "Occupancy grid mapping: An empirical evaluation," in *2007 mediterranean conference on control & automation*, pp. 1–6, IEEE, 2007.
- [21] L. Matthies and A. Elfes, "Integration of sonar and stereo range data using a grid-based representation," in *Proceedings. 1988 IEEE International Conference on Robotics and Automation*, pp. 727–733, IEEE, 1988.
- [22] S. B. Thrun, "Exploration and model building in mobile robot domains," in *IEEE international conference on neural networks*, pp. 175–180, IEEE, 1993.
- [23] S. Thrun, "Learning occupancy grid maps with forward sensor models," *Autonomous robots*, vol. 15, pp. 111–127, 2003.
- [24] T. Chan and W. Zhu, "Level set based shape prior segmentation," in *2005 IEEE Computer Society Conference on Computer Vision and Pattern Recognition (CVPR'05)*, vol. 2, pp. 1164–1170, IEEE, 2005.
- [25] C. Dapogny and P. Frey, "Computation of the signed distance function to a discrete contour on adapted triangulation," *Calcolo*, vol. 49, pp. 193–219, 2012.
- [26] A. Muller, "Energy optimal control of serial manipulators avoiding collisions," in *Proceedings of the IEEE International Conference on Mechatronics, 2004. ICM'04.*, pp. 299–304, IEEE, 2004.
- [27] A. Dosovitskiy, G. Ros, F. Codevilla, A. Lopez, and V. Koltun, "Carla: An open urban driving simulator," in *Conference on robot learning*, pp. 1–16, PMLR, 2017.
- [28] R. Rajamani, *Vehicle dynamics and control*. Springer Science & Business Media, 2011.